



## A robust spread spectrum based image watermarking in ridgelet domain

Hamidreza Sadreazami<sup>a,\*</sup>, Marzieh Amini<sup>b,1</sup>

<sup>a</sup> Department of Electrical Engineering, Shahid Beheshti University, 1983963113 Tehran, Iran

<sup>b</sup> Department of Electrical Engineering, Semnan University, Semnan, Iran

### ARTICLE INFO

#### Article history:

Received 25 April 2010

Accepted 6 September 2011

#### Keywords:

Digital image watermarking

Finite ridgelet transform

Spread spectrum technique

### ABSTRACT

A new robust method of spread spectrum based image watermarking is proposed in this article. Spread spectrum technique and scrambling are used for increasing robustness and invisibility of the algorithm. Our suggested method is carried out using ridgelet transform as an efficient transform for representing images with line singularities. In embedding part, the host image is partitioned into non-overlapping blocks and ridgelet transform is applied to each single block. In this way, a curved edge is divided into some straight edges so that ridgelet transform shows optimal performance even for complicated images with curve edges. To embed the watermark bits, the best directions of ridgelet coefficients are selected with respect to their variance intensity. In extraction part, a computationally efficient detection method is used for detecting watermark logo blindly from distorted watermarked image. To achieve more robust algorithm firstly, we find the best place to insert the watermark bits and secondly, we encode the scrambled watermark bits by pseudo random sequences with an authentication key. Robustness of our proposed method is tested against different kinds of attacks. According to the experimental results, proposed method shows much improved performance in comparison to other published works.

© 2011 Elsevier GmbH. All rights reserved.

### 1. Introduction

Watermarking is a way of embedding a key into the original data in order to increase security and copyright protection. Image watermarking algorithms are revolving around two categories based on the domain which is used for embedding the watermark: spatial and frequency domain techniques. Frequency domain techniques such as watermarking based on discrete cosine transform, discrete Fourier transform and digital wavelet transform are commonly used in recent works [1–6].

Although the discrete wavelet transform has strong performance for images with singularities in one dimension, point singularities, it does not provide good results for images with singularities in higher dimensions such as lines where are singularities in 2-D and planes where are singularities in 3-D. Ridgelet transform was introduced in [7–9] as a sparse expansion for functions which have discontinuities along lines but are otherwise smooth. Finite ridgelet transform (FRIT), an orthonormal version of ridgelet transform, was proposed in [10,11] for discrete and finite size images. Since ridgelet transform represents an image in small amount of space, it can be considered as an appropriate transform for digital watermarking.

Campisi et al. [12] proposed a multiplicative watermarking in ridgelet domain in which directional sensitivity and anisotropy of ridgelet transform are employed to obtain a sparse image representation. In their work, the most significant coefficients of ridgelet transform represent the most energetic direction of an image. Zhang et al. [13] proposed a multi scale ridgelet based watermarking algorithm in which watermark logo is embedded into middle ridgelet sub bands of the most energetic directions whose energies are greater than a selected threshold. Liang et al. [14], in their first work, proposed a ridgelet based perceptual model by computing the Just Noticeable Distortion for each ridgelet coefficient in order to consider the contrast and frequency sensitivity. This model combines a frequency detection threshold and a masking effect of human visual system. In their second work, Liang et al. [15] proposed the Noise Visible Function to control the strength of the watermark in each block. Also, a predefined peak signal to noise ratio (PSNR) is used for acquiring the global invisible parameter so that it would be guaranteed that the strength of the watermark in each block is proportional to the strength of the texture in that block. Kalantari et al. [16] proposed an image watermarking based on ridgelet transform in which a host distribution-independent decoder is used for extracting the watermark. Also, an analytical derivation of bit error rate (BER) is carried out in order to validate the empirical watermark extraction values. Li [17] proposed a combination of ridgelet transform with Kernel Independent Component Analysis (KICA). Watermark image is scrambled by Arnold method and then embedded into lowest sub band in ridgelet domain. In

\* Corresponding author. Tel.: +98 21 88757780.

E-mail address: [ha.sadreazami@mail.sbu.ac.ir](mailto:ha.sadreazami@mail.sbu.ac.ir) (H. Sadreazami).

<sup>1</sup> Tel.: +98 21 88825208.

extraction part, KICA is used for separating different mixed signals. All above works have concentrated on finding the best place for embedding the watermark. However, increasing the robustness of the watermarking algorithms is still developing.

In this paper, we propose a new watermarking algorithm in ridgelet domain which is based on spread spectrum technique. First, we find the best place to insert the watermark bits. More specifically, the host image is partitioned into several non-overlapping blocks in a way that curved edges appear as several straight edges. After applying ridgelet transform, we find a direction with the highest variance intensity for each single block in order to insert the watermark bits. Second, we encode the scrambled watermark bits by pseudo random sequences which are randomly generated through a uniform probability density function. Through comparison, we show that our proposed algorithm is highly robust against many kinds of attacks such as JPEG compression, rotation, Gaussian noise, median and Gaussian filtering,

The rest of this paper is organized as follow: in Section 2, a brief review of ridgelet transform and finite ridgelet transform are presented. In Section 3, embedding and extraction steps of proposed method are explained. Experimental result and discussion are presented in Section 4.

## 2. Ridgelet transform

### 2.1. Continuous ridgelet transform

The two-dimensional continuous ridgelet transform (CRT) for a given function  $I$  in  $\mathfrak{R}^2$  is defined as

$$CRT_I(a, b, \theta) = \int_{\mathfrak{R}^2} \psi_{a,b,\theta}(x, y) I(x, y) dx dy \quad (1)$$

In which, for each scale  $a > 0$  and  $(\theta, b)$  are the line parameters. Ridgelets are constant along ridge lines  $x \cos \theta + y \sin \theta = b$ , and cross section along the orthogonal directions which are wavelets. Also, a bivariate ridgelet function  $\psi_{a,b,\theta} : \mathfrak{R}^2 \rightarrow \mathfrak{R}^2$  is expressed as

$$\psi_{a,b,\theta}(x, y) = a^{-1/2} \psi \left( \frac{x \cos \theta + y \sin \theta - b}{a} \right) \quad (2)$$

The CRT can be calculated by performing wavelet transform in the Radon domain. The Radon transform is defined as [18]

$$R_I(\theta, t) = \int_{\mathfrak{R}^2} I(x, y) \delta(x \cos \theta + y \sin \theta - t) dx dy \quad (3)$$

where  $\delta$  is the Dirac delta function. Then ridgelet transform is obtained by applying the 1-D wavelet transform to the slice of Radon transform.

$$CRT_I(a, b, \theta) = a^{-1/2} \int_{\mathfrak{R}} \psi \left( \frac{t-b}{a} \right) R_I(\theta, t) dt \quad (4)$$

On top of that, a fast ridgelet transform can be carried out in Fourier domain as shown in Fig. 1. There should be noticed that ridgelet coefficients obtained in this way are not represented in Fourier frequency domain. Here, Fourier transform is only a tool to achieve a fast implementation of the ridgelet transform. In this method, first the 2-D fast Fourier transform (FFT) is computed. Then the samples of the Fourier transform on the square lattice are substituted with samples on a polar lattice. The 1-D inverse FFT is applied to each angular line. In order to obtain ridgelet coefficients, the 1-D wavelet transform is used.

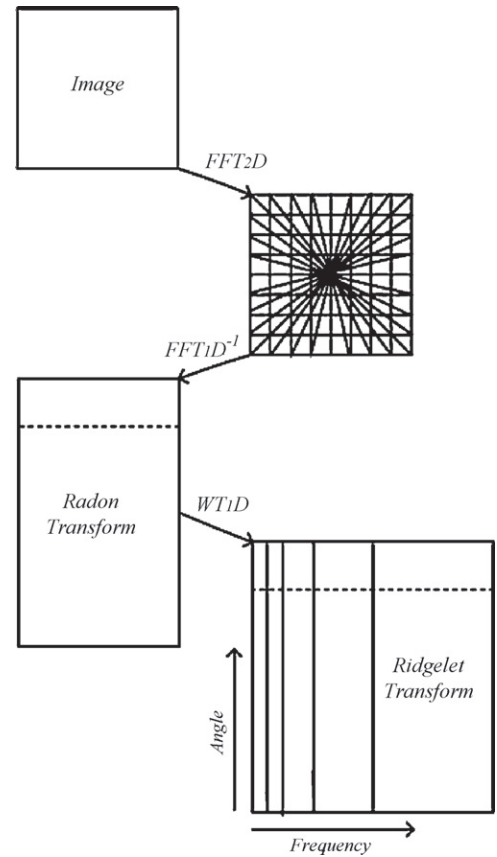


Fig. 1. Discrete ridgelet transform flowchart. Each radial line in Fourier domain is separately processed. The 1-D inverse FFT is calculated along each radial line followed by the 1-D wavelet transform.

### 2.2. The finite ridgelet transform

The finite ridgelet transform (FRIT), proposed in [11], is developed on the basis of finite radon transform (FRAT) as shown in Fig. 2. The FRAT of the real valued function on the 2-D grid  $Z_p^2$  is defined as

$$r_k[l] = FRAT_I(k, l) = \frac{1}{\sqrt{p}} \sum_{(i,j) \in L_{k,l}} I(i, j) \quad (5)$$

Here  $I(i, j)$  is the pixel value of the image at position  $(i, j)$ ,  $p$  is a Fermat prime number in the form of  $p = 2^k + 1$  and  $L_{k,l}$  is the set of points that form a line in the lattice of  $Z_p^2$  in which  $Z_p = \{0, 1, 2, \dots, p-1\}$  is a finite field.

$$L_{k,l} = \begin{cases} \{(i, j) : j = ki + l \pmod{p}, i \in Z_p\}, & 0 \leq k \leq p-1 \\ \{(l, j) : j \in Z_p\}, & k = p \end{cases} \quad (6)$$

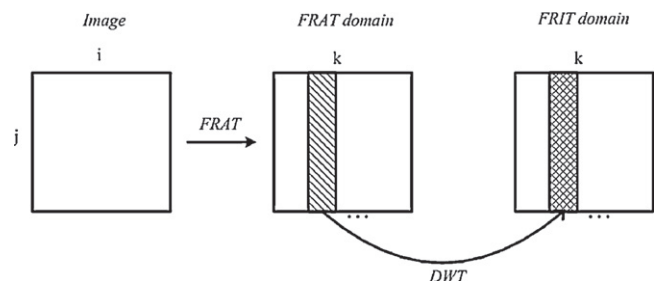


Fig. 2. Diagram of computing FRIT.

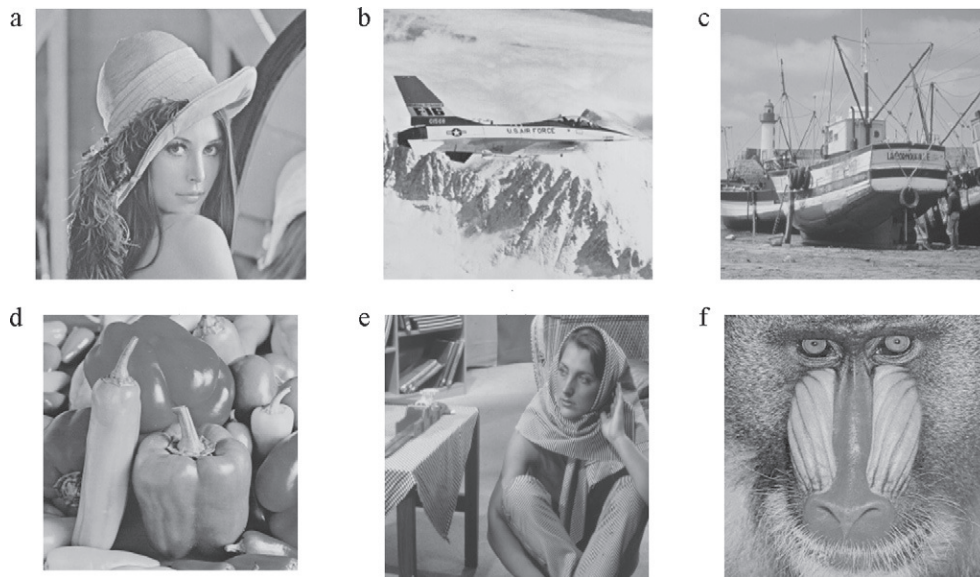


Fig. 3. Original images: (a) Lena, (b) Airplane, (c) Boat, (d) Pepper, (e) Barbara, and (f) Baboon.

where  $k=p$  corresponds to the vertical line. By taking the 1-D discrete wavelet transform on FRAT projection sequences denoted as  $(r_k[0], r_k[1], r_k[2], \dots, r_k[p-2])$  and for each direction of  $k$ , FRIT coefficients are obtained.

### 3. Embedding process

We assume the grayscale host image denoted by  $I$  of size  $N \times N$  and digital binary logo denoted by  $W$  of size  $M \times M$ . The watermark first is scanned to a 1-D sequence. It can be presented in binary form as  $W_i \in \{-1, 1\}$ . The pseudo random (PN) sequence elements  $\zeta$  are random numbers assuming  $-1$  or  $1$  according to a uniform, zero mean probability density function. The PN sequences of the set  $\zeta$  should be orthogonal to each other. The initial value of the PN sequence is an authentication key for generally assumed watermark logo. The watermark bits are passed through a scrambler in order to disseminate data in whole space and increase robustness

of the watermarking algorithm. The spread spectrum watermark sequence  $W_{ss}$  is derived from (7).

$$W_{ss}(1 : M, i) = W(i) \cdot \zeta(1 : M, i), \quad 1 < i < M^2 \quad (7)$$

In which the size of  $\zeta$  must be  $M \times M^2$ . The use of ridgelet transform is efficient for straight edges so that we split the original image into several non-overlapping blocks in a way that curved edges are divided into several straight edges. In our proposed algorithm, the original image is divided into  $B$  blocks of  $P \times P$ .

$$I(x, y) = \bigcup_{b=1}^B I_b(x', y'), \quad 1 \leq x', y' \leq P \quad (8)$$

The more number of curved edges in an image, the more number of non-overlapping blocks is needed. However, other restrictions are imposed to the number of blocks. For instance, each single block size of  $P \times P$  should be chosen in a way that  $P$  be a prime number and  $P-1$  be dyadic. Then, the FRIT is applied to each single block.

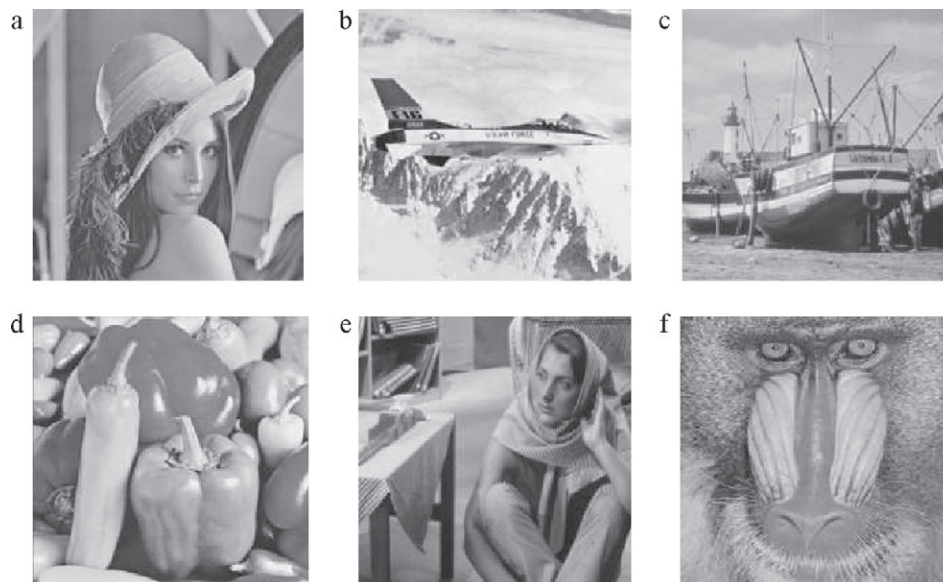


Fig. 4. Watermarked images: (a) Lena, (b) Airplane, (c) Boat, (d) Pepper, (e) Barbara, and (f) Baboon.

The matrix  $A$  is FRIT coefficients of each block whose size depends on both filter order and decomposition level of the 1-D wavelet.

$$A = \text{FRIT}_{l_b}, \quad 1 \leq b \leq B \quad (9)$$

In matrix  $A$ , each column represents one of the directions in ridgelet domain. In order to embed the coded watermark bits, variance of each column in matrix  $A$  is calculated. The column with maximum variance is considered as the best direction in ridgelet domain for inserting the watermark. It can be formulated as in (10).

$$l_b = \max_l (\text{var}(\text{FRIT}_{l_b}(1 : P + 1, l))) \quad (10)$$

which  $B = M^2$  and  $F_b$  is the matrix of selected directions for  $b$ th block.

$$F_b = [\text{FRIT}_{l_b}[1, l_b], \text{FRIT}_{l_b}[2, l_b], \dots, \text{FRIT}_{l_b}[P + 1, l_b]]^T, \quad 1 \leq b \leq B \quad (11)$$

Then selected columns are placed in matrix  $F$  in the same order as their blocks.

$$F = [F_1, F_2, \dots, F_B] \quad (12)$$

The proposed embedding equation is

$$F_w = F_b + \alpha \cdot F_b \cdot W_{ss} \quad (13)$$

where  $\alpha$  is scaling factor which is selected by compromising between similarity of original and extracted watermark and also PSNR of the watermarked image. The more scaling factor value, the lower visibility of the embedded watermark image is. Watermarked image is obtained by applying the inverse FRIT.

#### 4. Extraction process

The watermark extraction is the inverse process of watermark embedding. As for practical applications the host image is not accessible, the proposed algorithm is a blind watermarking method in which the host image is not required in extraction process. Given a corrupted image  $I^*$ , faced a certain type of attack, firstly the ridgelet transform is applied to each single block obtained from the same block partitioning of the watermarked image. The coefficients belonging to the best directions regarding their variance intensity are selected. These selected directions are successively placed in ridgelet coefficient matrix  $F_b^*$ . To put each coefficient in its own place, descrambling is done. An estimate of the original watermark is then obtained by multiplying each column with correspond PN sequence and its secret key followed by averaging all the copies of the same watermark bit. This averaging operation is used for smoothing possible modifications of the image.

$$X_s^*(j) = \frac{1}{M} \sum_{i=1}^M F_b^*(i, j) \cdot \underline{C}(i, j) \quad (14)$$

For a blind extraction, the correlation method needs to be employed between  $X_s^*$  and  $Y$  that can be original watermark sequence or a possibly different mark to compute the detector response.

$$z = \frac{1}{M^2} \sum_{j=1}^{M^2} X_s^*(j) \cdot Y(j) \quad (15)$$

By comparing  $z$  parameter obtained from some sample marks  $Y$ , the original watermark is experimentally obtained. In order to measure the effect of each attack, the extracted watermark sequence  $W^*$  is directly obtained from (16).

$$W^*(j) = X_s^*(j) \cdot W(j), \quad 1 < j < M^2 \quad (16)$$

Then the watermark image is reconstructed by scanning order.



Fig. 5. (a) Watermark logo and (b) extracted logo with NC=1 for all host images.

#### 5. Experimental results and discussion

To verify the proposed algorithm, we have tested it on some images. The  $510 \times 510$  grayscale Lena, Airplane, Boat, Pepper, Barbara and Baboon are chosen in following simulation in order to evaluate the proposed method and make a comparison with other published results. Watermark image is binary logo of size  $30 \times 30$ . The partitioning step is to ensure that data would be uniformly hidden throughout the host image. The host image is divided into  $B = 900$  blocks of  $17 \times 17$  pixels. As described in Section 3,  $N$  must be a prime number and  $N - 1$  must be dyadic. Due to the FRIT limitations, 17 is the best value for block size. A pseudo random number generator is used for producing a zero-mean sequence with an initial number as its secret key for each watermark image. Then watermark embedding is done by employing the method described in Section 3.

The original and watermarked images are shown in Figs. 3 and 4, respectively. Also, original watermark and extracted logos are shown in Fig. 5. For all original images, the watermark logo can be perfectly extracted. In order to compare the extracted,  $W^*$  and reference watermark logo  $W$ , normalized correlation (NC) can be defined as in (17).

$$NC = \frac{\sum_{i=1}^M \sum_{j=1}^M W(i, j) \cdot W^*(i, j)}{\sqrt{\sum_{i=1}^M \sum_{j=1}^M W(i, j)^2} \cdot \sqrt{\sum_{i=1}^M \sum_{j=1}^M W^*(i, j)^2}} \quad (17)$$

PSNR between original and watermarked images is computed to evaluate the imperceptibility of the algorithm and results are listed in Table 1 along with comparison to other published results. Dash lines show no experiment for specific images. Table 1 implies that the proposed watermarking algorithm provides substantial improvement in terms of invisibility of the embedding watermark.

In the following, the results of evaluating the proposed watermarking algorithm against a range of common attacks are presented.

##### 5.1. JPEG compression

JPEG algorithm is one of the most important attacks that watermark should be resistant to. JPEG compression is applied to the watermarked images for different quality factors. PSNR and BER of the corrupted images are compared to results from [16] in Table 2. According to results in Table 2 our proposed algorithm has better transparency and robustness. Fig. 6 compares normalized correlation for images: Lena, Baboon, Boat and Pepper detecting by proposed algorithm. It can be pointed out that the proposed method is considerably robust against image compression and watermark can be well detected for all images after facing JPEG compression

Table 1 Comparison of PSNR values in proposed watermarking method and other methods in [13–16].

	Proposed method	[13]	[16]	[14,15]
Lena	48.87	40.46	45	39.34
Airplane	46.31	38.05	–	–
Boat	48.01	38.34	45	–
Pepper	48.49	–	45	–
Barbara	51.08	40.14	–	–
Baboon	48.51	37.60	45	–



**Table 2**

PSNR and BER comparison between our proposed method and method in [16] for host images in the presence of JPEG compression with JPEG quality factors from 5 to 30.

		JPEG compression									
		5		10		15		20		30	
		Proposed method	[16]	Proposed method	[16]	Proposed method	[16]	Proposed method	[16]	Proposed method	[16]
Lena	PSNR	29.52	26.76	31.87	29.53	33.88	30.93	35.46	31.82	40.01	33.02
	BER	21.73	22.27	8.54	9.24	1.63	1.95	1.43	1.74	0.67	0.78
Boat	PSNR	27.92	26.04	29.70	28.86	31.50	30.36	32.44	31.42	35.80	32.85
	BER	22.81	23.30	8.93	9.64	2.43	3.52	1.47	1.56	0	0.39
Pepper	PSNR	29.24	27.44	32.34	30.15	33.85	31.41	34.63	32.13	35.91	32.99
	BER	20.39	21.22	7.98	8.07	3.27	4.56	1.99	2.21	0.59	0.78
Baboon	PSNR	26.75	23.72	28.70	26.77	29.99	28.65	30.32	29.95	35.21	31.82
	BER	18.73	19.01	5.94	7.03	1.54	1.69	0.17	0.26	0	0.13

with quality factor equal to 35. As can be seen in Fig. 6, Baboon image has the best performance for image compression in terms of robustness since it has more edges than other images. In other words, due to the use of ridgelet transform, better performance will be achieved for images with more curved edges. Watermarked images and extracted watermark logos are also displayed in Table 3 for Lena image against JPEG compression with different quality factors.

5.2. Rotation

Watermarked images are tested for geometric attack of rotation. Robustness of each host image is tested under rotation attack and results are listed in Table 4. It can be seen that Barbara image has the best performance against rotation attack. To compare our results with other published results, angle range is chosen between  $2^\circ$  and  $-2^\circ$ . In Fig. 7, BER for proposed method and results from [16,19] are plotted. According to Fig. 7, the proposed method exhibits better robustness to rotation attack. Extracted watermark logos are shown in Table 5 with different rotation angles.

5.3. Median filtering and Gaussian filtering

Robustness of proposed watermarking algorithm is evaluated against median filtering attack. Having been faced median filtering attack with different mask sizes on watermarked Lena image, extracted watermark is shown in Table 6.

In Fig. 8, normalized correlation of extracted watermark for some host images are displayed. As can be seen in Fig. 8, the median filtering attack has the least effect on Pepper image and watermark is substantially detected. Table 7 presents the PSNR comparison

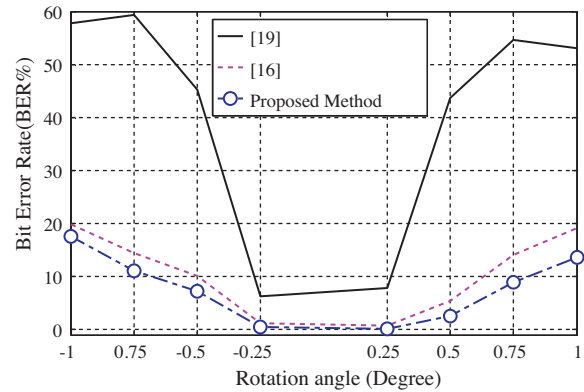


Fig. 7. BER comparison between our proposed algorithm and results in [16,19] under rotation attack for Lena image.

between our watermarking scheme and methods in [16,19] under median filtering attack with different mask sizes. As can be seen, our proposed watermarking scheme has better performance against median filtering attack in terms of transparency. In Table 8, result of detecting the watermark logo in the presence of Gaussian filter with filter size of  $3 \times 3$  and variable variance is presented. Results show that our proposed algorithm can considerably detect the watermark after facing Gaussian filtering. In Fig. 9, normalized correlation of extracted watermark as a robustness parameter for some host images are plotted. Pepper image has more smooth area than other images, it is more robust against attacks like Gaussian and median filtering. Baboon image, however, has the worst performance in the presence of Gaussian and median filtering attacks because of having more texture area. In Fig. 10, we compare our results with results

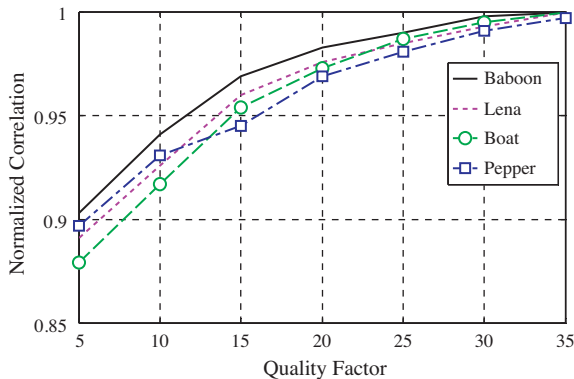


Fig. 6. Robustness of the proposed algorithm, NC values, in the presence of JPEG compression with different quality factors.

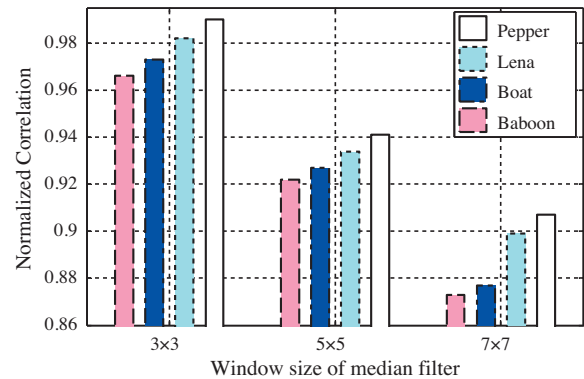


Fig. 8. Robustness of proposed algorithm, NC values, for Lena, Pepper, Boat and Baboon images against median filtering with mask size of  $3 \times 3$ ,  $5 \times 5$  and  $7 \times 7$ .

**Table 3**  
Extracted watermark logo for watermarked Lena image in the presence of JPEG compression.

Quality factor	Watermarked image	Extracted watermark
5		 NC= 0.887
10		 NC=0.926
15		 NC=0.960
20		 NC=0.975
25		 NC=0.985
30		 NC=0.994
35		 NC= 1

in [16] in the face of Gaussian filtering to show the robustness of proposed method.

5.4. Gaussian noise

In Fig. 11, the robustness of proposed algorithm in the presence of Gaussian noise for Lena image is compared to methods in [16,19]. The mean of the additive Gaussian noise is considered to be zero and its variance is variable. This comparison clearly demonstrates that our watermarking method outperforms the method in

**Table 4**  
Robustness of proposed watermarking method, NC values, under rotation attack.

Rotation angle (°)	Lena	Baboon	Pepper	Boat	Barbara	Airplane
-2	0.744	0.739	0.742	0.753	0.763	0.747
-1	0.873	0.861	0.872	0.878	0.881	0.853
-0.75	0.902	0.902	0.899	0.909	0.911	0.889
-0.5	0.937	0.928	0.932	0.943	0.946	0.921
-0.25	0.995	0.983	0.983	0.996	0.996	0.978
0.25	0.997	0.980	0.983	0.997	0.998	0.978
0.5	0.970	0.956	0.961	0.975	0.977	0.952
0.75	0.929	0.905	0.912	0.931	0.935	0.898
1	0.882	0.870	0.877	0.888	0.897	0.867
2	0.764	0.758	0.761	0.771	0.783	0.756





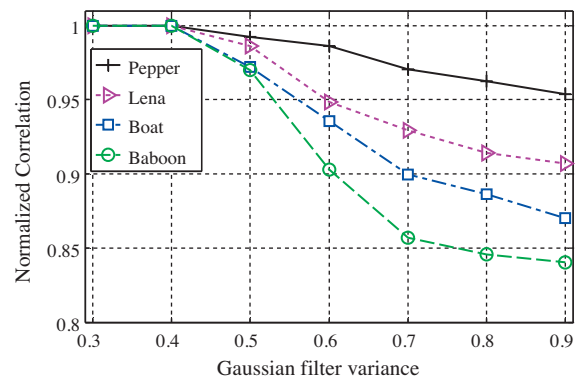


**Table 5**  
Extracted watermark logo for watermarked image of Lena under rotation attack.

Rotation angle (°)	Watermarked image	Extracted watermark
0.25		 NC= 0.997
0.5		 NC= 0.970
0.75		 NC= 0.929
1		 NC= 0.882



**Fig. 9.** Robustness, NC values, of proposed algorithm against Gaussian filtering with variance from 0.3 to 0.9 and mask size of 3 × 3 for Pepper, Lena, Boat and Baboon images.

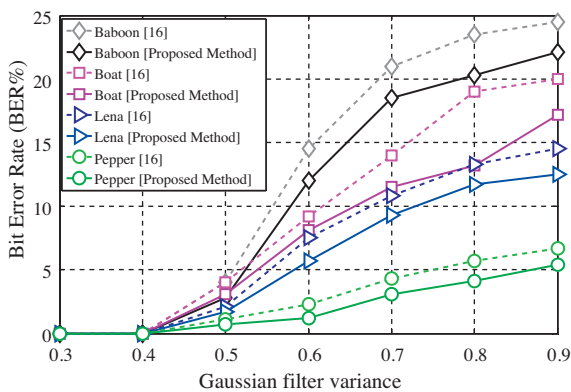
**Table 6**  
Extracted watermark logo for Lena image under median filtering with mask size of  $3 \times 3$ ,  $5 \times 5$  and  $7 \times 7$ .

Window size of median filter	Watermarked image	Extracted watermark
$3 \times 3$		 NC= 0.982
$5 \times 5$		 NC=0.934
$7 \times 7$		 NC= 0.899

**Table 7**  
PSNR comparison between our proposed algorithm and results in [16,19], under median filtering attack with various mask sizes.









Median filtering	Image	Proposed method	[16]	[19]
$3 \times 3$	Lena	40.68	33.67	30.46
	Baboon	35.11	29.80	26.97
	Pepper	41.54	33.24	29.67
$5 \times 5$	Lena	36.80	29.77	30.79
	Baboon	30.07	24.57	26.75
	Pepper	37.97	31.20	30.02
$7 \times 7$	Lena	33.37	27.66	30.66
	Baboon	27.17	22.58	26.52
	Pepper	34.63	29.59	29.73

[19] under Gaussian noise attack. For low noise variances our proposed method is as robust as method in [16]. However, there is a little difference between our proposed method and Ref. [16], in case of BER, for variances more than 10. The extracted watermark images obtained using proposed method are shown in Table 9 after











**Fig. 10.** BER comparison between our proposed method and method in [16] for Lena, Boat, Pepper and Baboon images against Gaussian filtering with variance from 0.3 to 0.9 and mask size of  $3 \times 3$ .

**Table 8**  
Extracted watermark logo for Lena image under Gaussian filtering with mask size of  $3 \times 3$  and different variances.

Gaussian filter variance	Watermarked image	Extracted watermark
0.3		 NC= 1
0.5		 NC= 0.986
0.7		 NC= 0.909
0.9		 NC= 0.901

**Table 9**  
Extracted watermark logo for Lena image under Gaussian additive noise with different variances.

Gaussian noise variance	Watermarked image	Extracted watermark
0.1		 NC= 0.999
0.2		 NC= 0.961
0.3		 NC= 0.924
0.4		 NC= 0.879

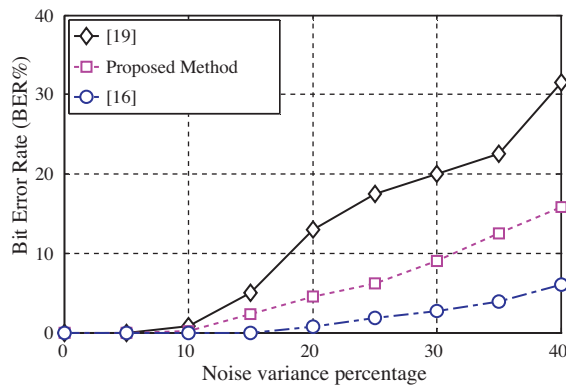


Fig. 11. Comparison of BER in proposed watermarking method and methods in [16,19] under Gaussian additive noise with different variances.

adding Gaussian noise with different variances. Although there are more attacks that can be tested, the results presented here give a good indication of the capabilities of the proposed method. Since the proposed watermarking algorithm takes advantage of ridgelet transform and spread spectrum technique simultaneously, the extracted watermark logos are more robust against all mentioned attacks. Consequently, both PSNR values of watermarked images and the robustness against attacks show considerable improvement using the proposed algorithm.

## 6. Conclusion

A new blind spread spectrum based watermarking in ridgelet domain is presented. Spread spectrum technique is used for increasing the robustness of the algorithm, along with scrambling. Watermarking process is commenced with partitioning the original image into several non-overlapping blocks so that we can efficiently use ridgelet transform characteristics for straight edges in each single block. Concerning variance intensity of each direction, ridgelet coefficients matrix is built by selecting the best directions to embed the watermark bits. Experimental results show no visible difference between host and watermarked images. Since our proposed algorithm takes advantage of both spread spectrum technique and ridgelet transform characteristics, the extracted watermark is considerably robust. To show the superiority of our proposed method, we compare our results with other published works. Through

comparison, it can be observed that our proposed method is showing high robustness to attacks such as JPEG compression, rotation, Gaussian noise, median and Gaussian filtering.

## References

- [1] Mehul R, Priti R. Discrete wavelet transform based multiple watermarking scheme. In: Proceeding of IEEE, Technical Conference on Convergent Technologies for the Asia-Pacific Bangalore, 2003. p. 14–7.
- [2] Ng TM, Garg HK. Maximum-likelihood detection in DWT domain image watermarking using Laplacian modeling. *IEEE Signal Processing Letter* 2005;12:345–8.
- [3] Reddy AA, Chatterji BN. A new wavelet based logo-watermarking scheme. *Pattern Recognition Letters* 2005;26:1019–27.
- [4] Dugad R, Ratakonda K, Ahuja N. A new wavelet based scheme for watermarking images. In: ICIP 98 Processing International Conference on 1998, vol. 2. 1998. p. 419–23.
- [5] Barni M, Bartolini F, Cappellini V, Piva A. A DCT domain system for robust image watermarking. *Signal Processing* 1998;66:357–72.
- [6] Loukhaoukha K, Chouinard JY. A new image watermarking algorithm based on wavelet transform. In: CCECE '09 Canadian Conference on Electrical and Computer Engineering. 2009. p. 229–34.
- [7] Candes EJ, Donoho DL. Ridgelet: a key to higher-dimensional intermittency. *Philosophical Transactions of the Royal Society of London* 1999: 2495–509.
- [8] E.J. Candes, Ridgelets: theory applications, Ph.D. dissertation. Dept. Statistics, Stanford Univ., Stanford, CA, 1998.
- [9] Starck JK, Candes E, Donoho DL. The curvelet transform for image denoising. *IEEE Transactions on Image Processing* 2002;11:670–84.
- [10] Do MN, Vetterli M. Orthonormal finite ridgelet transform for image compression. *International Conference on Image Processing* 2000;2: 367–70.
- [11] Do MN, Vetterli M. The finite ridgelet transform for image representation. *IEEE Transactions on Image Processing* 2003;12:16–28.
- [12] Campisi P, Kundur D, Neri A. Robust digital watermarking in the ridgelet domain. *IEEE Signal Processing Letters* 2004;11: 826–30.
- [13] Zhang Z, Yu H, Zhang J, Zhang X. Digital image watermark embedding and blind extracting in the ridgelet domain. *Journal of Communication and Computer USA* 2006;3:75–81.
- [14] Liang X, Zhihui W, Huizhong W. Embedding image watermarks into local linear singularity coefficients in ridgelet domain. *Lecture notes in computer science Berlin/Heidelberg: Springer; 2006. p. 119–27.*
- [15] Liang X, Zhihui W, Huizhong W. Ridgelet-based robust and perceptual watermarking for images. *IJCSNS International Journal of Computer Science and Network Security* 2006;6:194–201.
- [16] Kalantari NK, Ahadi SM, Vafadoost M. A robust image watermarking in the ridgelet domain using universally optimum decoder. *IEEE Transaction on Circuits and Systems for Video Technology* 2010;20:396–406.
- [17] Li Y. An image digital watermarking method based on ridgelet and KICA. *International Conference on Multimedia and Information Technology* 2008;3:345–8.
- [18] Deans SR. *The radon transform and some of its applications*. New York: Wiley; 1983.
- [19] Bi N, Sun Q, Huang D, Yang Z, Huang J. Robust image watermarking based on multiband wavelets and empirical mode decomposition. *IEEE Transactions on Image Processing* 2007;16:1956–66.